



HAL
open science

Intrinsic timescales of variability in a marine plankton model

Benjamin Mayersohn, K. Shafer Smith, Inès Mangolte, Marina Lévy

► **To cite this version:**

Benjamin Mayersohn, K. Shafer Smith, Inès Mangolte, Marina Lévy. Intrinsic timescales of variability in a marine plankton model. *Ecological Modelling*, 2021, 443, pp.109446. 10.1016/j.ecolmodel.2021.109446 . hal-03111008

HAL Id: hal-03111008

<https://hal.science/hal-03111008>

Submitted on 15 Jan 2021

HAL is a multi-disciplinary open access archive for the deposit and dissemination of scientific research documents, whether they are published or not. The documents may come from teaching and research institutions in France or abroad, or from public or private research centers.

L'archive ouverte pluridisciplinaire **HAL**, est destinée au dépôt et à la diffusion de documents scientifiques de niveau recherche, publiés ou non, émanant des établissements d'enseignement et de recherche français ou étrangers, des laboratoires publics ou privés.

Intrinsic timescales of variability in a marine plankton model

Benjamin Mayersohn^{a,b}, K. Shafer Smith^{a,b,*}, Inès Mangolte^c, Marina Lévy^c

^a*Courant Institute of Mathematical Sciences, New York University, New York, New York 10012, USA*

^b*Center for Prototype Climate Modeling, New York University, Abu Dhabi, UAE*

^c*Sorbonne Université (CNRS/IRD/MNHN), Laboratoire d’Océanographie et du Climat (LOCEAN), Institut Pierre, Simon Laplace (IPSL), Paris Cedex 05 75252, France*

Abstract

Phytoplankton are known to exhibit temporal variability in biomass and community composition. While physically driven sources of variability have been studied extensively, ecosystems often exhibit complicated intrinsic dynamics that are not as well understood. As a first step towards assessing the contribution of this intrinsic variability to the total variability in the ocean, we examine the temporal scales of intrinsic variability in a marine plankton model suitable for use in climate model projections. Our rationale is that a better understanding of the time scales over which intrinsic variability manifests could help in the attribution of observed variability. Our model includes multiple phytoplankton, dissolved inorganic nutrients, and zooplankton and supports two oscillatory mechanisms: “R-oscillations”, corresponding to patterns of species succession and associated with changes in resources, and “Z-oscillations”, corresponding to changes in total phytoplankton biomass due to predator-prey interactions.

Over a wide range of model parameters, we found that while Z-oscillations typically occurred on time scales not exceeding 60 days, R-oscillations ranged from roughly 100 to 900 days under predation-free conditions, and R-oscillations occurred on longer time scales when interacting with Z-oscillations. Thus the two kinds of oscillations can be easily distinguished. At high grazing rates, we identified aperiodic cases where the dominant period never resolved, with distinct regimes emerging over decadal (or longer) time scales. These chaotic regime shifts are likely highly dependent on the model parameters and structure. More work must be done to understand how these oscillations interact with physical forcings.

Keywords: Intrinsic variability, phytoplankton, predator-prey dynamics

1. Introduction

Phytoplankton communities exhibit different temporal modes of variability both in total biomass and community structure. Understanding the drivers of this natural variability is a prerequisite for confidently identifying changes in the ecosystem attributable to anthropogenic forcing. Ocean color observations of chlorophyll-a (a proxy for phytoplankton biomass), for example, have revealed variability at intraseasonal (weeks to months), seasonal, and interannual (> 1 year) time scales over most open ocean regions (Behrenfeld et al., 2006; Martinez et al., 2009; Resplandy et al., 2009; Vantrepotte and Mélin, 2011; Thomalla et al.,

*Corresponding author at: Courant Institute of Mathematical Sciences, New York University, New York, New York 10012, USA. *Email address:* kss3@nyu.edu

8 2011; Demarcq et al., 2012; Mayot et al., 2017; Salgado-Hernanz et al., 2019; Keerthi et al., 2020; Huisman
9 et al., 2006). In-situ measurements of phytoplankton species abundances, as well as observations from ocean
10 color remote sensing (which has been used to infer phytoplankton functional types and sizes), reveal that
11 community structure varies over a similar range of time scales to chlorophyll-a (Alvain et al., 2008; d’Ovidio
12 et al., 2010; Demarcq et al., 2012; Rousseaux and Gregg, 2015; Mayot et al., 2017; Dakos et al., 2009). This
13 wide range of time variability in phytoplankton communities is also seen in global biogeochemical models of
14 the ocean (Aumont et al., 2018; Dutkiewicz et al., 2019).

15 Much of the variability found in marine phytoplankton communities can be attributed to variability in
16 the physical environment in which they evolve. A typical example is the spring phytoplankton bloom, which
17 is driven by seasonal changes in light and vertical mixing (Platt et al., 2009; Sathyendranath et al., 2015, and
18 references therein), and which explains the largest part of the time variability (Demarcq et al., 2012). At
19 the intraseasonal timescale, variability can be driven by intraseasonal basin-scale climate modes such as the
20 Madden-Julian oscillation (Resplandy et al., 2009), synoptic atmospheric forcing due to storms (Fauchereau
21 et al., 2011; Carranza and Gille, 2014) and tropical cyclones (Menkes et al., 2016), or by oceanic mesoscale
22 and submesoscale processes acting at even smaller spatial scales (Mahadevan et al., 2012; Lévy et al., 2018;
23 Poggiale et al., 2013; Keerthi et al., 2020). At lower frequencies (interannual to multidecadal timescales), part
24 of the variability is forced by large-scale, low-frequency climate modes such as the Pacific Decadal Oscillation,
25 the El Niño Southern Oscillation or the Atlantic Multidecadal Oscillation (Chavez et al., 2011, and references
26 therein).

27 However, phytoplankton also exhibit complex dynamics even in the absence of external variability. Empir-
28 ical evidence for such intrinsic variability is difficult in the natural environment because the external forcing
29 is always present. However, it can be seen in dedicated laboratory experiments where the experimental condi-
30 tions are artificially held constant. For example, Fussmann et al. (2000) have demonstrated the potential
31 for predator-prey oscillations in a culture with one nutrient, one phytoplankton species and one zooplankton
32 species in a continuous flow-through chemostat. More recently, predator-prey oscillations have been observed
33 to persist over several predator-prey cycles in a controlled culture of planktonic rotifers and unicellular green
34 algae in the laboratory (Blasius et al., 2019; Hastings, 2020). Benincà et al. (2008) conducted a long-term (>
35 8 years) laboratory mesocosm experiment with a more complex plankton food web (two nutrients and ten
36 functional groups) that exhibited striking fluctuations of different periodicities (from 15 days to 225 days),
37 attributable only to interactions between species in the food web.

38 Phytoplankton intrinsic variability is a recurrent topic in theoretical ecology. Limit cycles — and some-
39 times chaos (Benincà et al., 2015) — in phytoplankton populations are emergent properties of mathematical
40 models of interspecies interactions. These models, usually constructed to represent a system in a chemostat
41 under constant conditions (Gothlich and Oschlies, 2015), have shown that internal variability may result
42 from two fairly different processes: competition between different phytoplankton species for limiting re-
43 sources (Tilman, 1977; Huisman and Weissing, 1999, 2001) and predator-prey interactions (Gilpin, 1979;
44 Edwards and Brindley, 1996). The zero-dimensional food web models developed for these ecological studies
45 are similar to the ones used for global biogeochemical studies, where the plankton equations are solved in
46 three dimensions and are embedded into an ocean circulation model. We might therefore expect internal

47 variability to manifest in these forced 3D models.

48 In the natural environment, it is difficult to disentangle internal variability from forced variability. An
49 improved understanding of phytoplankton intrinsic variability is a prerequisite to confidently identify the
50 phytoplankton trends attributable to physical forcings, which are likely to dominate in the open ocean (and
51 in 3D models of the open ocean) but might not explain all of the observed variability. As a first step towards
52 assessing how much intrinsic variability in phytoplankton biomass and community structure contributes to
53 the total variability in the ocean, our objective is to examine the temporal scales of intrinsic variability in a
54 marine plankton model. A better understanding of the time scales over which intrinsic variability manifests
55 could help in the attribution of observed variability.

56 In this study, we focus on the two types of intrinsic variability mentioned previously: those due to
57 competition between phytoplankton for multiple resources, which we call R-oscillations, and those due to
58 predator-prey interactions, which we call Z-oscillations. These two kinds of oscillations have been studied in
59 isolation, but never together to our knowledge. Here we ask specifically: (1) what are the time scales for each
60 type of oscillation, (2) how do they interact, and (3) what is their sensitivity to a realistic range of model
61 parameters? To address these questions, we have developed a moderately-complex ecosystem model that
62 supports both kinds of intrinsic variability, and we use it to explore the time scales of variability that emerge
63 under constant environmental forcing in a chemostat system. The closest analogue of our chemostat scenario
64 to a physical regime is a low-latitude eastern boundary upwelling region, such as the Benguela ([Messié et al.,](#)
65 [2009](#)). High nutrient delivery via upwelling, combined with relatively low seasonality due to its proximity to
66 the equator, provide an optimal environment for any existing mechanisms of intrinsic variability to persist.
67 The present paper can be considered the first entry in a two-part study; the second step will be to investigate
68 how these intrinsic variations manifest under time-varying external forcings.

69 A key goal in constructing our model is to bridge the gap between highly idealized conceptual mod-
70 els focused on specific ecological interactions, and the much more complex biogeochemical components of
71 Earth-system models used for global climate simulations. The latter class of models achieved a milestone
72 with [Fasham et al. \(1990\)](#), who developed a nitrogen-based biogeochemical model used in a General Circula-
73 tion Model for the North Atlantic Ocean ([Sarmiento et al., 1993](#)), and [Aumont et al. \(2003\)](#), who investigated
74 the effect of multi-nutrient limitation on the biological carbon pump. Building from these first biogeochemical
75 models, the PISCES model ([Aumont et al., 2015](#)) was incorporated into the IPSL-CM5 earth system model
76 as part of CMIP5 ([Bopp et al., 2013](#)). The even-more-complex Darwin ecosystem model ([Follows et al., 2007](#))
77 was used by [Prowe et al. \(2014\)](#) to examine the effect of phytoplankton diversity on primary production in
78 response to environmental changes. Wherever possible, we follow common choices in the class of models
79 described above in determining model representations of processes and parameter values.

80 Section 2 introduces the model that we will use, including the equations and the numerical integration
81 scheme (a simplified version of the equations is also presented in [Appendix A](#)). Section 3 presents four
82 example simulations: two that exhibit each type of oscillation in isolation, and two that demonstrate the
83 complexity of the full model. Section 4 explores the sensitivity of the results to key parameters involved in
84 the phytoplankton growth and decay rates, using multidimensional sweeps over model parameters adding
85 up to 6400 separate simulations. The results demonstrate the emergent regimes arising from the underlying

86 oscillations. Finally in section 5 we discuss the implications of these results, in particular how the emergent
87 frequencies depend on the presence of and interaction between different kinds of oscillations. We discuss how
88 the time scales of intrinsic variability that emerges compares with time scales of external forcings in the open
89 ocean. Ideas regarding future experiments to address this topic are also presented.

90 2. A chemostat-like model for studying intrinsic variability

91 Here we develop a chemostat-like model, with a continuous inflow of nutrients and without variations
92 in light or temperature. This is arguably the simplest system that mimics a physical setting — something
93 roughly like a low-latitude Eastern boundary upwelling system (see e.g. [Messié et al. \(2009\)](#)), with a high rate
94 of nutrient influx from the deep ocean and relatively low seasonality — yet permits only variability driven
95 by internal dynamics. The model shares common terms with other biogeochemical models, and all ecological
96 parameters are assigned reasonable values based on the literature. While our model does support oscillatory
97 behavior that is not common in other models, we believe that these features are reasonably explained by the
98 general complexity of ecosystem dynamics.

99 To represent the dynamics discussed in the introduction, the model requires multiple nutrient, phyto-
100 plankton and zooplankton compartments. [Huisman and Weissing \(2001\)](#) have shown that R-oscillations
101 start emerging when the number of species and the number of resources is equal or larger than three. And
102 of course, Z-oscillations require the presence of at least one phytoplankton and one zooplankton species. As
103 is common in biogeochemistry models of this kind (e.g. [Dutkiewicz et al., 2009](#); [Aumont et al., 2015](#)), we
104 include two size classes for phytoplankton: small species (gleaners) that thrive in nutrient-poor environments,
105 and larger species (opportunists) that dominate in nutrient-rich environments.

106 Given these constraints, we therefore include two phytoplankton size classes with three phytoplank-
107 ton each, for six phytoplankton in total: P_1^s through P_3^s are small species, while P_1^l through P_3^l are large
108 species. The different phytoplankton compartments within the same size class represent distinct species (e.g.
109 prochlorococcus and synechococcus are both picophytoplankton), rather than members of the same species
110 with different ecological properties. Two species of zooplankton are also included: Z^s is a microzooplankton
111 species that consumes small phytoplankton, while Z^l is a larger mesozooplankton species that consumes
112 both large phytoplankton and microzooplankton. The model includes three dissolved inorganic resource
113 compartments R_j , representative of nitrogen (R_1 , $\mu\text{mol}/\text{m}^3 \text{N}$), phosphorus (R_2 , $\mu\text{mol}/\text{m}^3 \text{PO}_4$), and iron
114 (R_3 , $\mu\text{mol}/\text{m}^3 \text{Fe}$). We restrict our model to three nutrients because it is the minimum number required to
115 produce R-oscillations. Iron is chosen over silicate because the need for silicate is specific to large diatoms.
116 Also, for simplicity, the model does not distinguish between different forms of nitrogen such as nitrate and am-
117 monium. Phytoplankton and zooplankton compartments have units $\mu\text{mol C}$, with stoichiometric conversions
118 for the phytoplankton compartments described below. The model is configured in a chemostat setting, with
119 relaxation of resource R_j toward target values S_j at a dilution rate τ . Biomass is removed through mortality
120 and via outflux at the same dilution rate τ ; explicit remineralization and settling are omitted. Phytoplankton
121 mortality is linear as is typical in these models ([Cropp and Norbury, 2009](#)). Quadratic zooplankton mortality
122 parameterizes density-dependent losses such as viral infection, and also acts as a closure term for predation

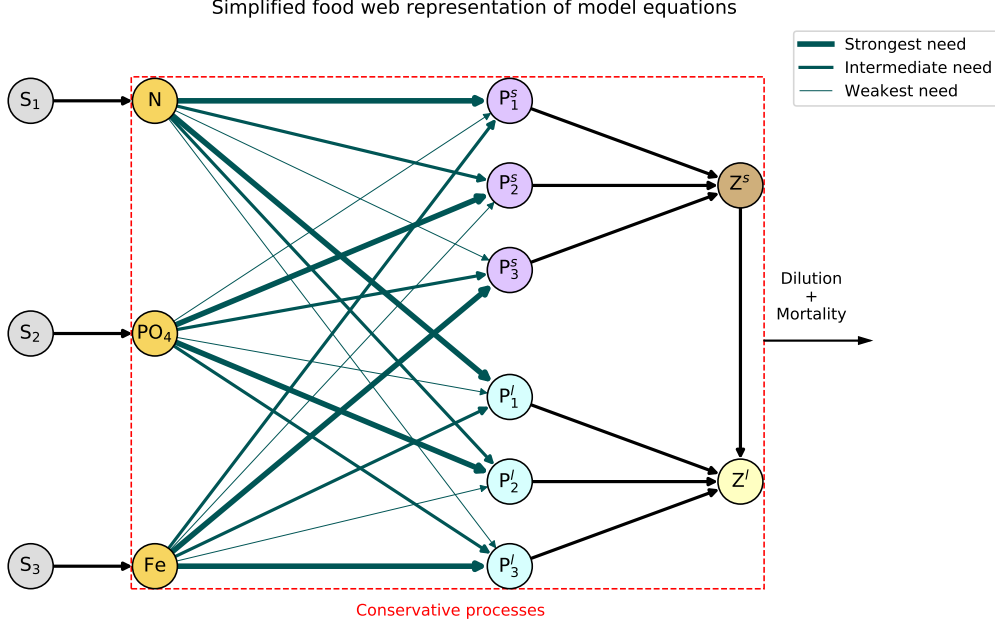


Figure 1: A food web representation of the model equations. Phytoplankton are controlled from the bottom-up by externally-supplied nutrients and from the top-down by zooplankton. The widths of the arrows pointing to a given phytoplankton depend on its relative needs for each nutrient. *Conservative processes*, or exchanges that do not result in any loss of mass from the system, are contained within the dashed red box. That is, without the deep nutrient supply; natural phytoplankton and zooplankton mortality terms; and loss of biomass through dilution, the system would exhibit biomass conservation.

123 by species unrepresented in this model (Aumont et al., 2015). A model schematic is shown in Figure 1. A
 124 simplified version of this model is provided in Appendix A.

125 *2.1. Model equations*

126 The model equations are

$$\frac{dR_j}{dt} = \tau(S_j - R_j) - \sum_{i=1}^3 C_{ji} \left[\mu^s \min_j \frac{R_j}{K_{ji}^s + R_j} P_i^s + \mu^l \min_j \frac{R_j}{K_{ji}^l + R_j} P_i^l \right], \quad (1a)$$

$$\frac{dP_i^s}{dt} = -\tau P_i^s + \left[\mu^s \min_j \frac{R_j}{K_{ji}^s + R_j} - m_P - \frac{g^s Z^s}{K_Z + P_{\text{tot}}^s} \right] P_i^s, \quad (1b)$$

$$\frac{dP_i^l}{dt} = -\tau P_i^l + \left[\mu^l \min_j \frac{R_j}{K_{ji}^l + R_j} - m_P - \frac{g^l Z^l}{K_Z + Z^s + P_{\text{tot}}^l} \right] P_i^l, \quad (1c)$$

$$\frac{dZ^s}{dt} = -\tau Z^s + \frac{g^s Z^s}{K_Z + P_{\text{tot}}^s} P_{\text{tot}}^s - \left[\frac{g^l Z^l}{K_Z + Z^s + P_{\text{tot}}^l} + m_Z Z^s \right] Z^s \quad (1d)$$

$$\frac{dZ^l}{dt} = -\tau Z^l + \frac{g^l Z^l}{K_Z + Z^s + P_{\text{tot}}^l} (Z^s + P_{\text{tot}}^l) - m_Z (Z^l)^2 \quad (1e)$$

127 where $i, j = 1, 2, 3$, and $P_{\text{tot}}^{s,l} = \sum_{i=1}^3 P_i^{s,l}$.

128 The phytoplankton growth rates are equal to a nutrient limitation factor scaled by the maximum growth
 129 rate μ . Nutrient limitation is set dynamically by the smallest Monod growth factor, which depends on the
 130 values of K_{ji} . Large phytoplankton species (opportunists) grow faster and require more nutrient than small
 131 phytoplankton species (gleaners), allowing the former to thrive in high-nutrient environments, and the latter

| Parameter | Default Value | Units | Description |
|--------------------------------------|-----------------------------------|--|--|
| τ | 0.04 | day ⁻¹ | Nutrient restoring rate ¹ |
| S_j | 18.1, 1.21, 1.21×10^{-3} | $[R_j]$ | Deep ocean nutrient source values ¹ |
| μ^s, μ^l | 0.308, 0.616 | day ⁻¹ | Maximum phytoplankton growth rates ² |
| m_P | 0.1 | day ⁻¹ | Phytoplankton mortality rate ² |
| r_j | 0.15, 0.01, 1×10^{-5} | $\frac{[R_j]}{\mu\text{mol}/\text{m}^3\text{C}}$ | Nutrient : Carbon ratios ³ |
| c_{\min}, c_{\max} | 0.9, 1.3 | | Stoichiometric scaling factors (Eq. 3) |
| $\kappa_j^s = \frac{1}{4}\kappa_j^l$ | 0.15, 0.01, 1×10^{-5} | $[R_j]$ | Nutrient uptake half-saturation constants ² |
| k_{\min}, k_{\max} | 0.7, 1.1 | | Nutrient half-saturation scaling factors (Eq. 4) |
| g^s, g^l | 1.5, 0.5 | day ⁻¹ | Grazing rates ⁴ |
| K_Z | 10 | $\mu\text{mol}/\text{m}^3\text{C}$ | Grazing half-saturation constant ⁴ |
| m_Z | 0.015 | $(\mu\text{mol}/\text{m}^3\text{C} \cdot \text{day})^{-1}$ | Zooplankton mortality rate ⁵ |

¹ Typical for the Benguela upwelling system (Messié et al., 2009)

² Follows et al. (2007)

³ $r_1 = \text{N:C}$, $r_2 = \text{PO}_4\text{:C}$, $r_3 = \text{Fe:C}$ (Redfield, 1934)

⁴ Aumont et al. (2015)

⁵ Messié and Chavez (2017)

Table 1: Definitions and default values for model parameters. Subscript $j = 1, 2, 3$. The notation $[R_j]$ means “the units of R_j ”, which are $[R_1] = \mu\text{mol N}$, $[R_2] = \mu\text{mol PO}_4$, and $[R_3] = \mu\text{mol Fe}$. References for default values are given where appropriate in footnotes.

132 to overtake competitors in low-nutrient environments. This is modeled by setting $\mu^l = 2\mu^s$ (see Table 1 for
 133 values) and $K_{ji}^l = 4K_{ji}^s$.

134 *2.2. Nutrient source, stoichiometry, and uptake limitation*

135 We set the nutrient source relaxation rate $\tau = 0.04 \text{ days}^{-1}$ and deep nitrogen concentration value $S_1 =$
 136 $18.1 \mu\text{mol N}$, which are characteristic of, for example, the Benguela upwelling system (Messié et al., 2009).
 137 The other deep nutrient concentrations are derived from S_1 through the Redfield ratios r_j (Table 1), i.e.

$$\frac{S_1}{r_1} = \frac{S_2}{r_2} = \frac{S_3}{r_3}. \quad (2)$$

138 The phytoplankton stoichiometric coefficients C_{ji} in the nutrient uptake term convert increases in biomass
 139 to corresponding losses in the inorganic nutrient pools; large and small phytoplankton share the same sto-
 140 ichiometry. The Redfield ratio is an average of the stoichiometry found across a variety of phytoplankton
 141 species (Klausmeier et al., 2004), and so we include some variation in the stoichiometry for each modeled
 142 species. The stoichiometry matrix C_{ji} is constructed such that for a given nutrient and phytoplankton group,
 143 one species has exactly the Redfield value, another species has a slightly larger value controlled by $c_{\max} > 1$,
 144 and the third species has a slightly smaller value controlled by $c_{\min} < 1$. Dividing each row by r_j , the matrix
 145 is

$$\frac{C_{ji}}{r_j} = \begin{pmatrix} c_{\max} & 1 & c_{\min} \\ c_{\min} & c_{\max} & 1 \\ 1 & c_{\min} & c_{\max} \end{pmatrix} \quad (3)$$

146 So for example, P_1 , P_2 , and P_3 have the largest, intermediate, and smallest stoichiometric values for nitrogen,
 147 respectively. This is reflected in Figure 1, with the thickness of the lines between the phytoplankton and
 148 nutrients corresponding to the magnitudes of the stoichiometric coefficients.

149 Half-saturation constants for a given nutrient and a specific size class (gleaners, say) are similar between
 150 species in that size class. Denoting $\kappa_j^{s,l}$ as the typical half-saturation value for resource j and size class s or l
 151 (See Table 1 for values), the half-saturation matrix has a similar structure to the stoichiometric matrix, with

$$\frac{K_{ji}^{s,l}}{\kappa_j^{s,l}} = \begin{pmatrix} 1 & k_{\min} & k_{\max} \\ k_{\max} & 1 & k_{\min} \\ k_{\min} & k_{\max} & 1 \end{pmatrix} \quad (4)$$

152 where $k_{\max} > 1$ and $k_{\min} < 1$ designate the entries with the largest and smallest coefficients per row (species),
 153 respectively.

154 *2.3. Model numerics and spinup*

155 The model is written in Python 3.6 and integrated in time with the SciPy `odeint` library (Millman and
 156 Aivazis, 2011). This module acts as a wrapper for ODEPACK’s LSODA solver that automatically switches
 157 between Adams (non-stiff) and BDF (stiff) integration methods when appropriate (Hindmarsh, 1982; Petzold,
 158 1983). The time series for each of the model compartments is stored in intervals of one day.

159 All simulations were run for 200 years, with the exception of one 500 year simulation to illustrate a
 160 longer-term phenomenon, depicted in Figure 6. We have observed that the spinup time for these simulations

161 is typically around 1-2 years. But because some of our simulations have very long periods of oscillation —
162 and may even exhibit aperiodic behavior — we took a conservative approach and only used the last 150 years
163 of each simulation for analysis.

164 3. Example simulations: Resource oscillations, predator-prey oscillations and their interactions

165 The model described above is designed to capture two primary mechanisms of intrinsic variability: competi-
166 tion between phytoplankton for resources (R-oscillations), and predator-prey interactions (Z-oscillations).
167 In this section we consider four basic example simulations. The first two are designed to understand the
168 nature of each oscillation independently. The *NoPred* simulation removes both zooplankton, in order to
169 highlight how resource competition can give rise to coexistence amongst phytoplankton in a similar size
170 class. The *SimpleCom* (for “simple competition”) case retains only two phytoplankton species, one from each
171 of the two size classes, thus allowing only predator-prey interactions. The third case, called *WeakPred*, is an
172 example of the full system that uses parameters given in Table 1. In this case, the two types of oscillations
173 are both present, but remain distinct enough to isolate in their time-series and frequency spectra. The last
174 case, termed *StrongPred*, employs increased grazing rates; the result is a simulation in which the types of
175 oscillations interact in complex ways, producing time series that exhibit broadband chaotic behavior.

176 3.1. Case *NoPred*: Isolated R-oscillations

177 The first example, which we call *NoPred*, removes predators from the model by disabling all terms that
178 contain Z^s and Z^l . Figure 2 shows time series and frequency spectra for the nutrients and small phytoplankton
179 species. The spectra were computed using the discrete Fourier transform (DFT) after centering the data
180 around zero and multiplying the remainder by a Hamming window. In the caption and throughout the paper,
181 we use the term “dominant period” to denote the reciprocal of the frequency with the largest amplitude in
182 the spectrum. If the dominant period is equal to the length of the series, then we say that the series has not
183 equilibrated and we do not assign a dominant period.

184 For this particular parameter regime, the large phytoplankton are not shown because they die out via com-
185 petitive exclusion. The large phytoplankton have higher growth rates, but larger half-saturation coefficients,
186 which means they require greater ambient nutrient concentrations to compete successfully with gleaners;
187 an increase in the nutrient input rate τ or deep nutrient concentrations S_j , for example, would lead to the
188 elimination of small phytoplankton instead. Peaks in the individual small phytoplankton alternate roughly
189 every 90 days. Every time an individual species peaks, one also sees peaks in both the total phytoplankton
190 P_{tot}^s and in the nutrient compartments. The correspondence between a peak in PO_4 and a peak in P_2^s (as
191 well as a peak in the total phytoplankton) is highlighted by the vertical red lines. The same correspondence
192 occurs between P_s^1 and N, and between P_s^3 and Fe. The oscillations of total phytoplankton biomass are small
193 compared with fluctuations in the individual compartments.

194 These R-oscillations are well described by the *resource-ratio hypothesis* of species succession (Tilman,
195 1985). Such oscillations depend on two factors: differences in the phytoplankton stoichiometric coefficients
196 C_{ji}/r_j (3) across the nutrient pools, and differences in the half-saturation coefficients K_{ji}/κ_j (4) between
197 species. The driving mechanism behind R-oscillations can be summarized in two steps:

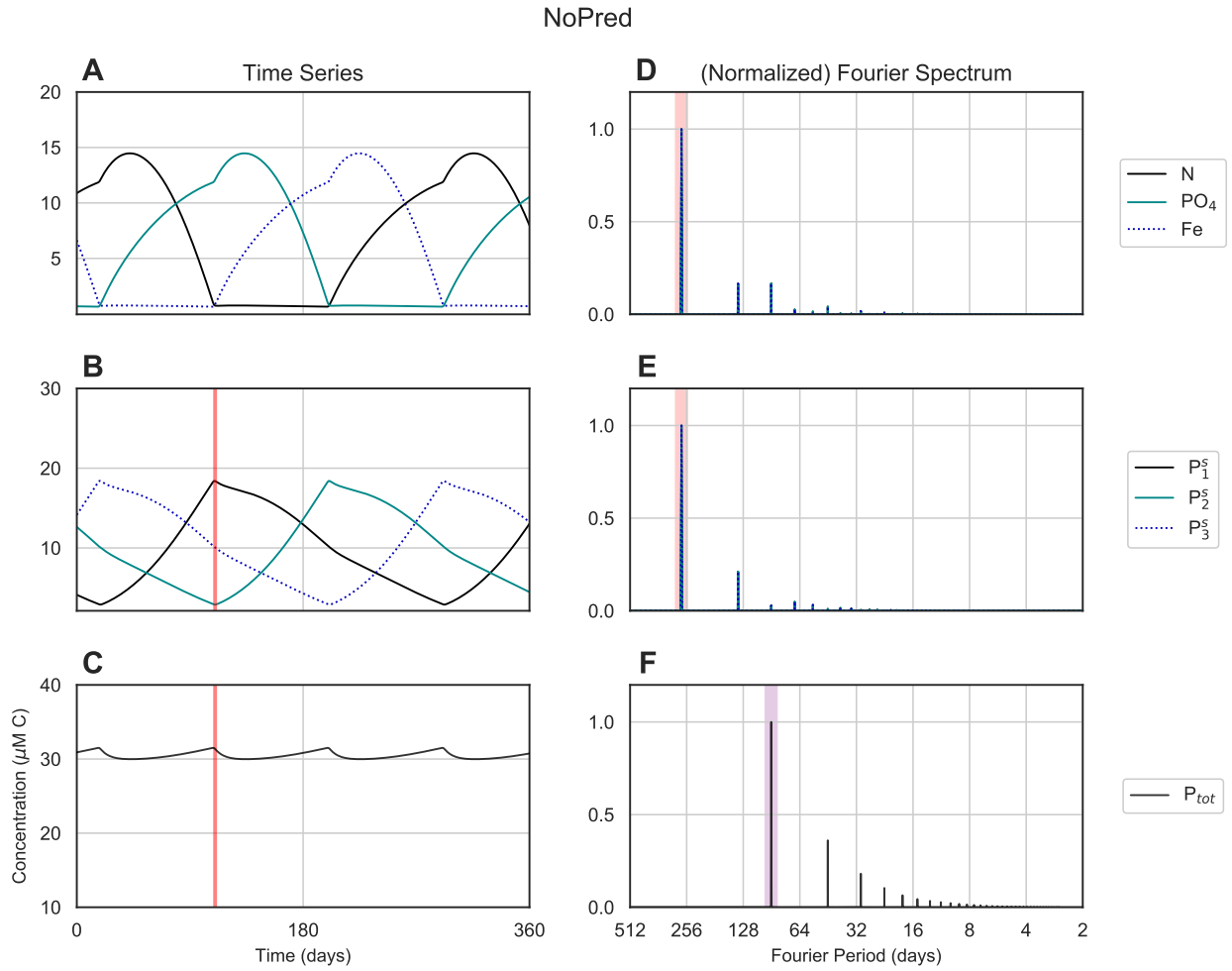


Figure 2: Time series of the last year (left column, panels A-C) and frequency spectra of the last 50 years (right column, panels D-F) from a 200 year simulation of the *NoPred* (isolated R-oscillations) scenario. The rows correspond to (top) nutrients, (middle) surviving phytoplankton (large phytoplankton do not survive in this scenario), and (bottom) total phytoplankton. See legends for curve identification. In panel B, the red vertical line corresponds to a peak in P_1^s , while the blue lines correspond to peaks in P_1^l . The purple lines in panel C correspond to peaks in the small and large zooplankton. These peak indicators were all copied into panel D to demonstrate that zooplankton peaks follow those of the phytoplankton. The red shading in panels D and E indicates the dominant periods for the phytoplankton and nutrients (all share the same peak at approx. 273 days), and the purple shading in panel F indicates the dominant period for the total phytoplankton (approx. 91 days).

- 198 1. The current dominant phytoplankton depletes the nutrient for which it has the largest C_{ji}/r_j , at a rate
 199 proportional to c_{\max} .
- 200 2. The phytoplankton with the largest growth rate at low values of the newly-depleted nutrient will become
 201 the next dominant phytoplankton. By construction, this phytoplankton is the one with the minimum
 202 half-saturation constant K_{ji}/κ_j (proportional to k_{\min}) for this given nutrient.

203 Let us say that P_1^s is dominant. For this phytoplankton, the largest nutrient need (largest C_{ji}/r_j) is for
 204 nitrogen. Thus, P_1^s depletes nitrogen first as it grows. This sets up P_2^s , which has the largest growth rate at
 205 low values of nitrogen (lowest K_{ji}/κ_j) compared with its competitors, to become the next dominant species.
 206 This two-step process repeats as P_2^s depletes phosphorus and P_3^s is primed to thrive when this nutrient is
 207 limiting. Finally, P_3^s depletes iron, allowing P_1^s to thrive and completing a full cycle. In this case, c_{\max}
 208 and k_{\min} are two key parameters that regulate this oscillatory mechanism. Increasing c_{\max} accelerates the
 209 depletion of what will become the next limiting nutrient in the system. Decreasing k_{\min} enhances the growth
 210 rate of the next dominant species, resulting in a faster invasion.

211 With the chosen parameter set, individual phytoplankton oscillations take about 273 days to complete,
 212 while total phytoplankton biomass cycles take one third as long (91 days) due to symmetries in the oscillations
 213 of the individual compartments; these symmetries emerge because the stoichiometric matrix (3) and half-
 214 saturation matrix (4) are circulant. Also, note that fluctuations in the total phytoplankton concentrations
 215 are relatively small compared to oscillations in the individual compartments. This is because R-oscillations
 216 primarily represent variability at the species level.

217 3.2. Case SimpleCom: Isolated Z-oscillations

218 The second example, which we call *SimpleCom*, is obtained by including both zooplankton, but just
 219 one large and one small phytoplankton with the same stoichiometric coefficients: P_1^s and P_1^l . In this case,
 220 nitrogen will always be the limiting nutrient, so the stoichiometric diversity that generates oscillations among
 221 competing species is removed, while predator-prey cycles are left intact.

222 While R-oscillations primarily represent variability at the species level, Z-oscillations are a form of total
 223 biomass variability that occurs when zooplankton growth rates are sufficiently large. They induce significant
 224 fluctuations in both the total phytoplankton and individual species concentrations. In panel G of Figure 3 we
 225 see that peaks in the zooplankton time series always follow peaks in the phytoplankton series. As is typical of
 226 a predator-prey model, zooplankton concentrations evolve in the direction of phytoplankton biomass changes,
 227 while phytoplankton concentrations evolve inversely to zooplankton biomass changes. In this case, because
 228 of the zooplankton size selectivity, the small and large phytoplankton alternate dominance. The large and
 229 small zooplankton alternate dominance as well, with each following peaks in their target prey. But small
 230 zooplankton are restricted to small bursts following peaks in small phytoplankton, as large zooplankton
 231 exhibit top-down control on their biomass. The dominant period of the total phytoplankton in this scenario
 232 is about 40 days. The dominant period of P_1^s is about 81 days, while the double-peaked large phytoplankton
 233 has a dominant period of about 27 days.

SimpleCom

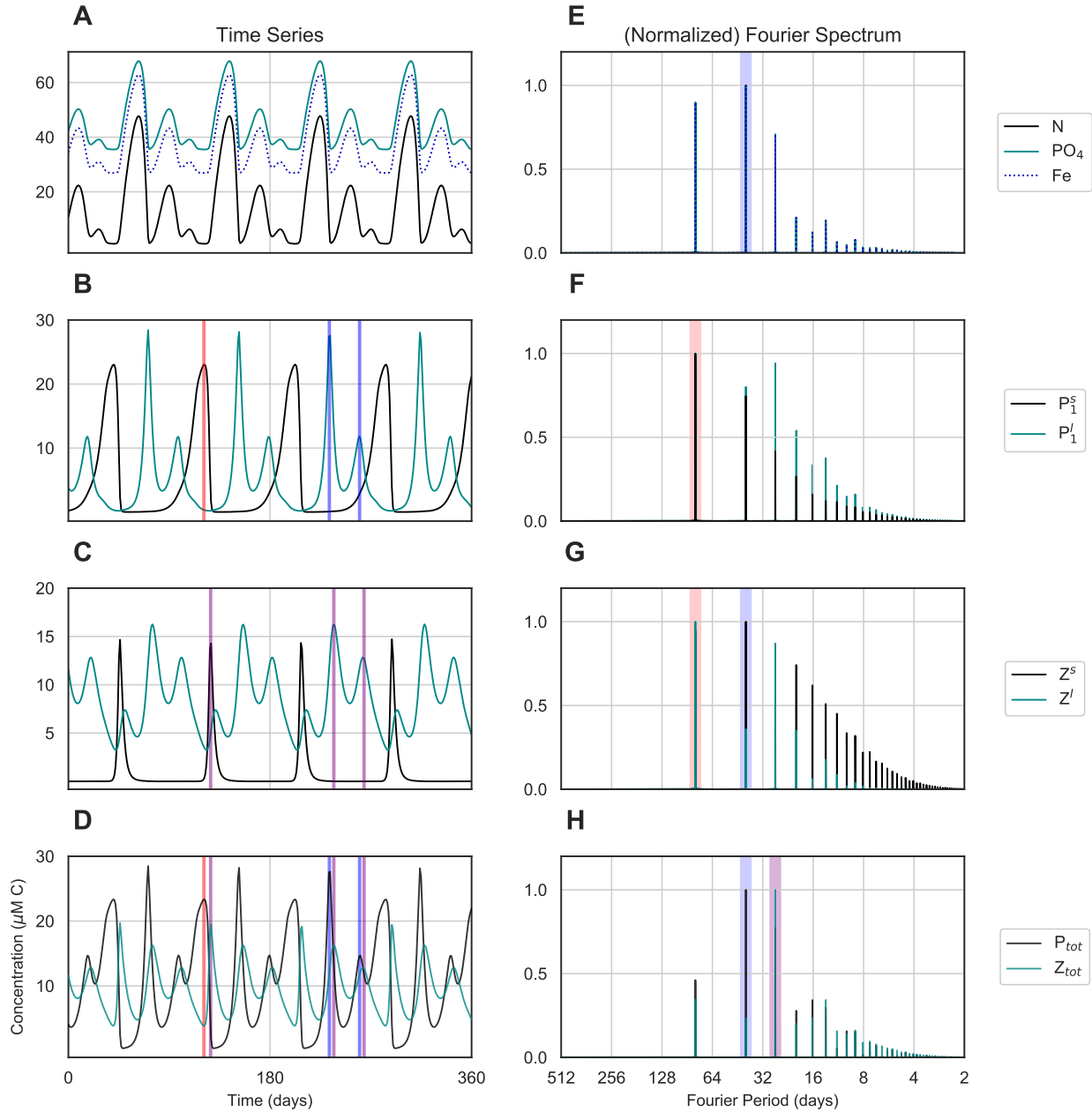


Figure 3: Time series of the last year (left column, panels A-E) and frequency spectra of the last 50 years (right column, panels F-J) from a 200 year simulation of the *SimpleCom* (isolated Z-oscillations) experiment. The rows correspond to (top) nutrients, (second) phytoplankton, (third) zooplankton, and (bottom) total phytoplankton and total zooplankton. See legends for curve identification. The red vertical line in panels B and C corresponds to a peak in P_1^s . In the spectra plots, dominant periods are indicated by: red shadings for individual phytoplankton and large zooplankton (approx. 81 days); blue shadings for nutrients, total phytoplankton, and small zooplankton (approx. 40 days); and purple shadings for nutrients and total phytoplankton (approx. 27 days).

WeakPred

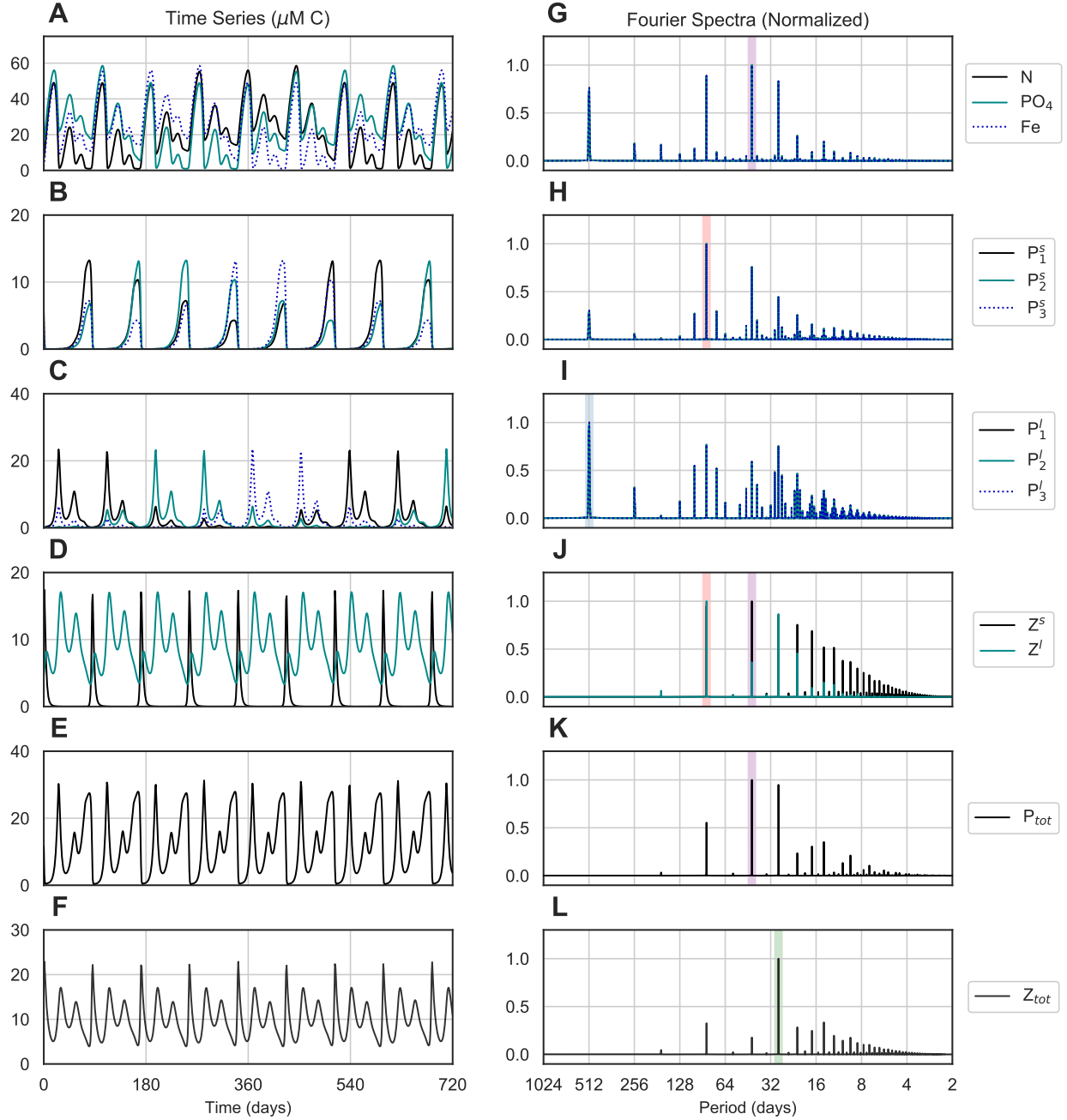


Figure 4: The time series (first column) and frequency spectra (second column) for phytoplankton, nutrient, and zooplankton compartments from a 200 year run of the *WeakPred* simulation. See legends for curve identification. The last two years of the time series are shown, and the last 150 years of the simulation were used to compute the spectra. In the spectra plots, dominant periods are indicated by: red shadings for the small phytoplankton and large zooplankton (approx. 85 days); blue shadings for the large phytoplankton (approx. 509 days); green shadings for the total zooplankton (approx. 28 days); and purple shadings for the total phytoplankton and small zooplankton (approx. 43 days).

234 *3.3. Case WeakPred: The full system with distinct R- and Z-oscillations*

235 Here we consider an example simulation in which all compartments of the full model equations (1) are
236 active, using the parameters given in Table 1. The results can be seen in Figure 4. From the plots of N ,
237 P_1^s and P_1^l , we see that both R- and Z-oscillations are present, and can be easily distinguished. The low
238 frequency peak in panel I, with a period of approximately 514 days, is indicative of R-oscillations: analogous
239 species P_1^s and P_1^l evolve together, while nitrogen is depleted and restored. A similar pattern exists between
240 phosphate, P_2^s and P_2^l , and amongst iron, P_3^s and P_3^l .

241 By contrast, the high frequency patterns of alternating dominance between the small and large phy-
242 toplankton resemble those of the *SimpleCom* simulation; the large phytoplankton exhibit a double-peaked
243 pattern, as before, while the small phytoplankton are single-peaked, with low concentrations of biomass away
244 from the peaks. And like in the *SimpleCom* simulation, peaks in the zooplankton series follow their phyto-
245 plankton counterparts. The dominant period of the total phytoplankton, whose peaks reflect those of the
246 alternating small and large phytoplankton, is 28 days.

247 *3.4. Case StrongPred: The full system with chaotic interactions*

248 In this last example, the grazing pressure is increased relative to the *WeakPred* simulation, with grazing
249 rates g^s, g^l set to 1.15 times the values given in Table 1. The result is a simulation that exhibits more
250 complex behavior, as shown by the time series and frequency spectra in Figure 5. The dominant period of
251 the total phytoplankton and zooplankton (purple vertical shading in spectra plots) is roughly 31 days, and
252 the dominant period of the nutrient and small zooplankton (green vertical shading) is roughly 64 days. There
253 are several properties that distinguish this scenario from the *WeakPred* case. First, the spectrum is much
254 more broadband, with dominant periods appearing more like clusters than individual peaks. Second, the time
255 series exhibits low frequency variations in amplitude that are not present in *WeakPred*: an entire *WeakPred*
256 cycle is visible within a two year window, whereas that is not the case for the *StrongPred* simulation. Third, in
257 *WeakPred* (and in *SimpleCom*), Z-oscillations take place between analogous small and large phytoplankton.

258 For the individual phytoplankton, the dominant period never resolves. The reason for this becomes clear
259 in Figure 6, which shows the last 50 years of an extended 500 year *StrongPred* run. The series exhibits
260 heteroclinic cycles of increasing periodicity until roughly 35 years into the plotted series (indicated by the
261 orange vertical line), where there is a marked shift in the phytoplankton and nutrient series. From this
262 point until the end of the run, P_1^l is present at a low concentration and continues to oscillate with the other
263 species. This regime shift indicates an aperiodicity in the series, making the Fourier decomposition a less
264 useful tool for understanding the nature of the oscillations. This is confirmed by looking at the frequency
265 spectra in panels D, E, and F (taken from the last 400 years of the 200 year run). We see that the spectrum
266 is quite broadband compared with the narrow high frequency peaks observed in previous simulations, shown
267 in Figures 4 and 5.

268 **4. Intrinsic time scales of community change**

269 In this section we use large sets of simulations to sample swaths of parameter space and explore the nature
270 of the emergent frequencies. Specifically, we vary a subset of parameters involved in the phytoplankton growth

StrongPred

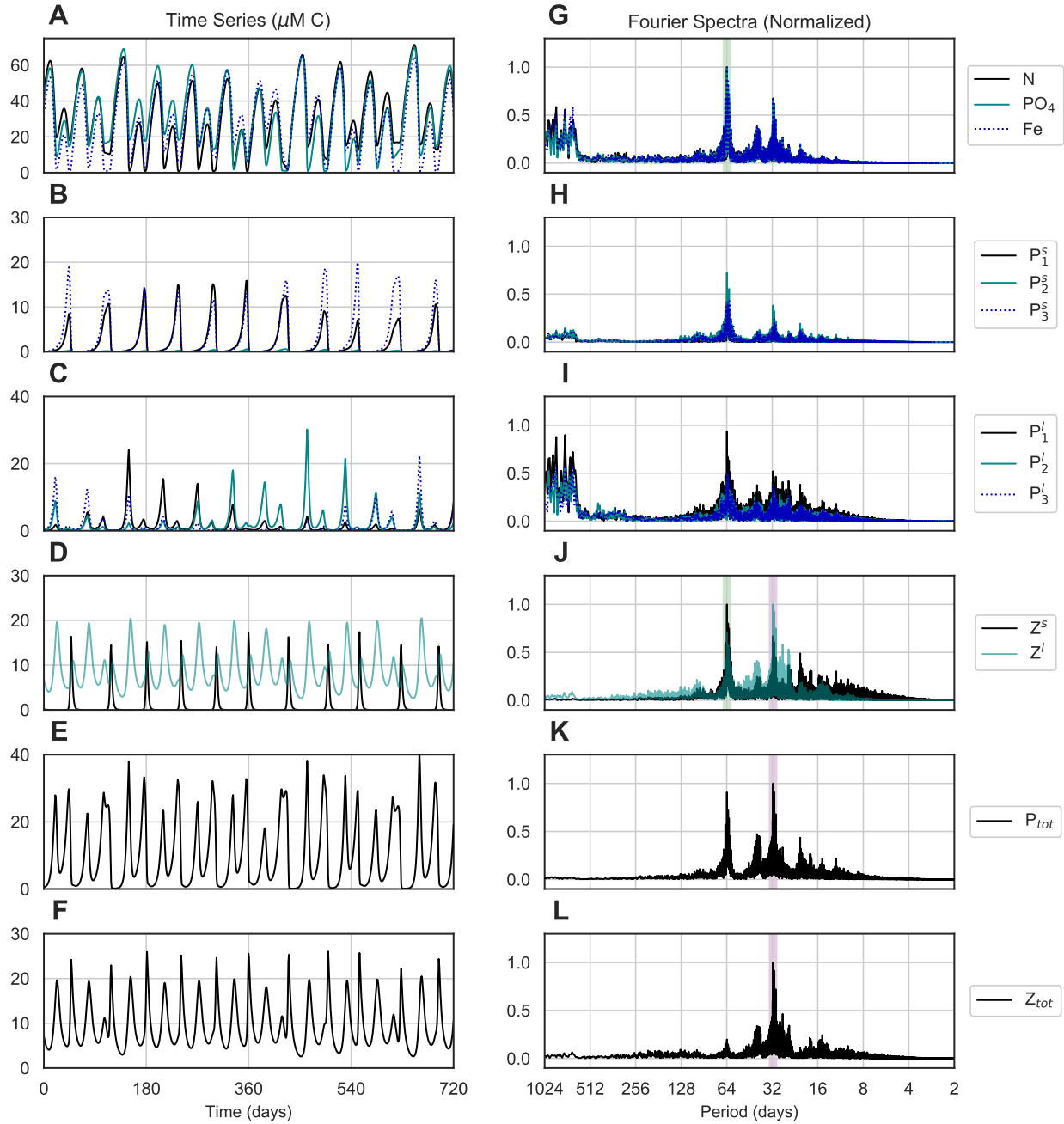


Figure 5: The time series and frequency spectra for the *StrongPred* simulation, with the same layout as for Figure 4. Two dominant periods occur at approximately 64 days for nutrients and small zooplankton (green shading) and 31 days for total phytoplankton and large/total zooplankton (purple shading). But there is also a low frequency component that does not fully resolve, as indicated by the lack of a dominant period in the individual phytoplankton spectra.

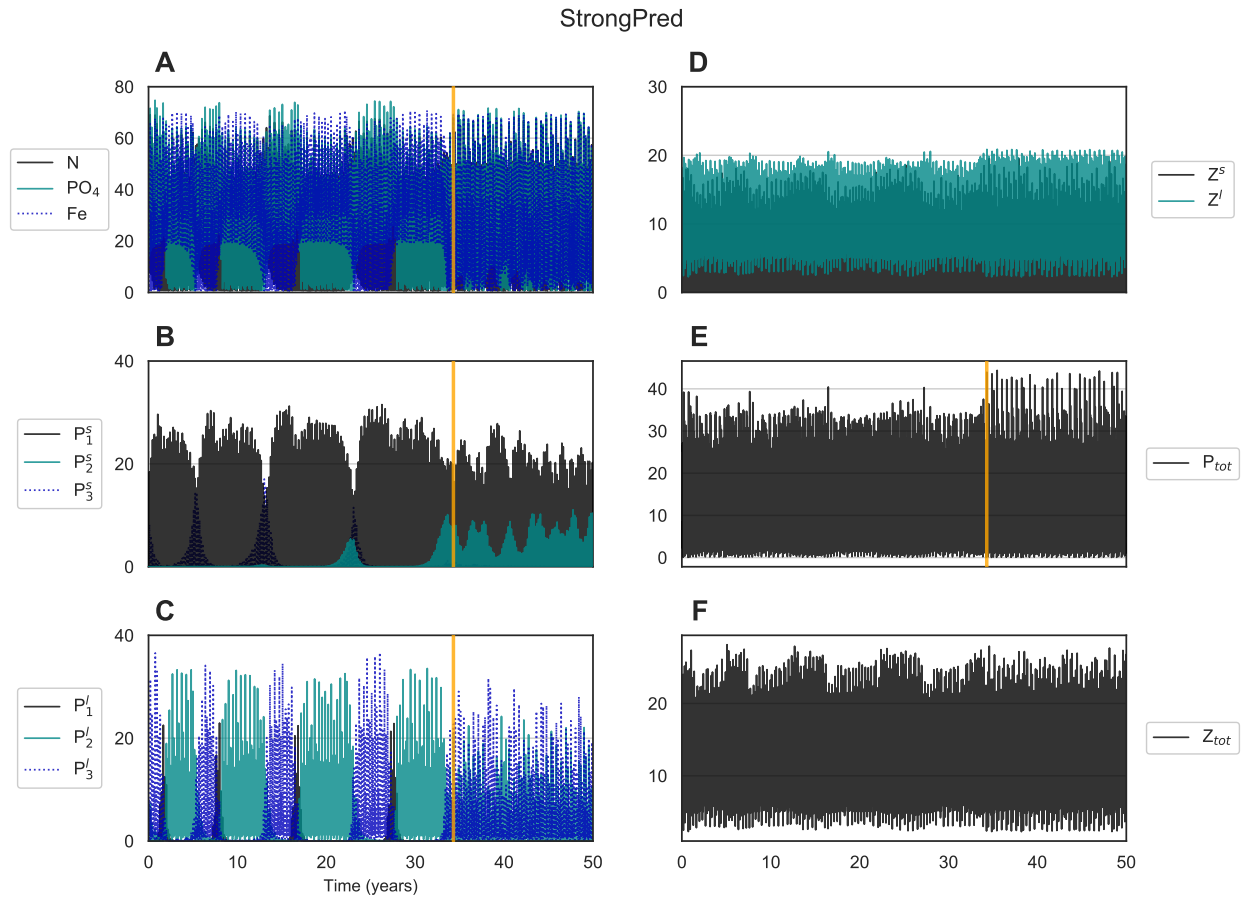


Figure 6: The last 50 years of an extended 500 year *StrongPred* simulation, highlighting a notable regime shift indicated by the orange vertical line. This shift is preceded by clear heteroclinic cycles, characterized by oscillations whose periods lengthen with each iteration, in the nutrient and phytoplankton compartments.

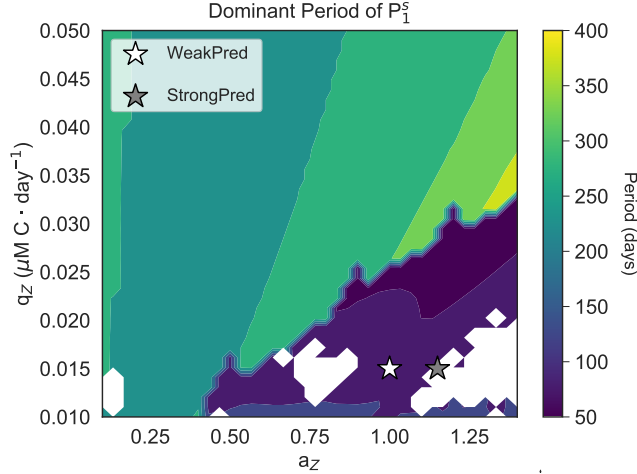


Figure 7: Dominant period for P_1^s as a function of zooplankton mortality m_Z and grazing rate scaling factor a_Z . There are three primary regimes: domination by slow R-oscillations; domination by fast Z-oscillations; and aperiodic regimes where the dominant period never resolves (shown in white).

271 and decay rates, i.e. grazing rates, zooplankton mortality rate, the nondimensional scaling factor c_{\max} for
 272 the stoichiometry matrix (3), and the nondimensional scaling factor k_{\min} for the half-saturation matrix (4).

273 We first focus on controlling Z-oscillations by varying the quadratic zooplankton mortality rate m_Z , and
 274 the grazing rates g^s and g^l . We used the same multiplicative coefficient a_Z to scale the large and the small
 275 grazing rate as $a_Z g^s$ and $a_Z g^l$ (e.g. the *StrongPred* example used $a_Z = 1.15$). The parameter range used for
 276 these sweeps is

$$0.01 \leq m_Z \leq 0.05 \quad \text{and} \quad 0.1 \leq a_Z \leq 1.5, \quad (5)$$

277 where recall that the values for m_Z have units $\mu\text{mol C day}^{-1}$. For each sweep, we assigned 40 possible
 278 linearly-spaced values per parameter, for a total of 1600 simulations. Each simulation was run for 200 years
 279 and the last 150 were used for analysis.

280 Figure 7 shows the dominant period of P_1^s as a function of m_Z and a_Z . There are three primary regimes:
 281 domination by slow R-oscillations; domination by fast Z-oscillations; and regimes where a dominant period
 282 never resolves over the 150 year period considered (shown in white). In the regime where R-oscillations
 283 dominate, the dominant period tends to increase with the grazing pressure. When zooplankton reduce
 284 phytoplankton biomass, they also reduce the rate at which the phytoplankton deplete nutrients. This increases
 285 the time it takes a new nutrient to become limiting and a new species to become dominant. Furthermore,
 286 the next dominant species invades at a slower rate because phytoplankton growth rates are inhibited. Thus,
 287 grazing interferes with the species succession mechanism.

288 We can better understand how enhanced grazing affects species succession by examining the dominant
 289 period over a range of saturation and stoichiometric coefficients. The time-scale of R-oscillations depends on
 290 the value of the parameters that control these oscillations, i.e. in our case c_{\max} and k_{\min} (refer to section 3.1
 291 for an explanation). To examine how these key parameters impact the frequency of oscillations, we started
 292 from the default set of parameters in Table 1 and varied them over a range that respects their constraints:

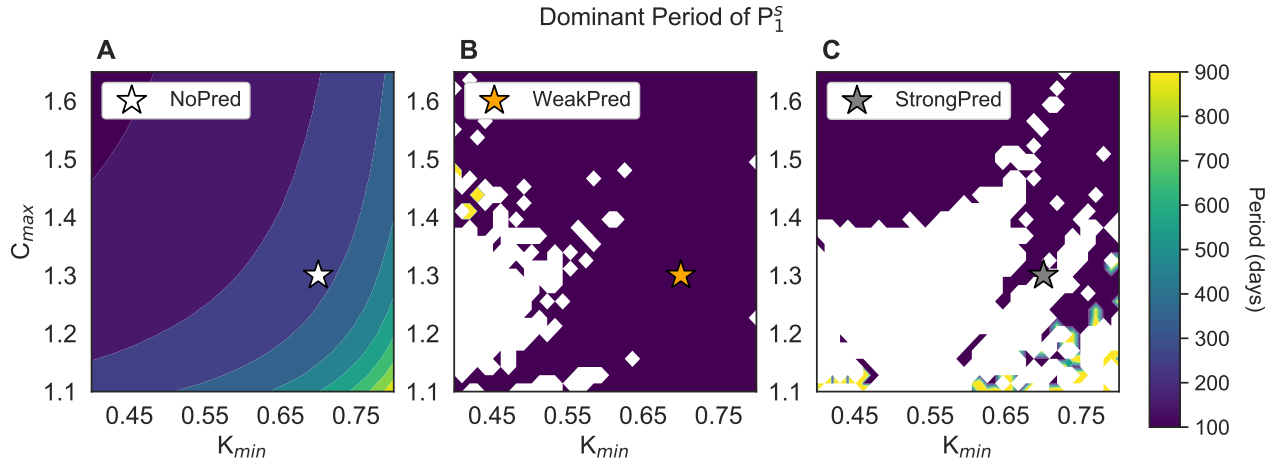


Figure 8: Dominant period of P_1^s for sweeps over c_{\max} and k_{\min} , in order of increasing grazing pressure from left to right. White regions indicate cases where no dominant period emerges, due to aperiodicity. As the grazing pressure increases, the dominant period is less likely to resolve over the considered range of parameters.

293 $k_{\min} < 1$ and $c_{\max} > 1$:

$$0.4 \leq k_{\min} \leq 0.8 \quad \text{and} \quad 1.1 \leq c_{\max} \leq 1.65. \quad (6)$$

294 The range chosen is just large enough to clearly illustrate the dependence on the parameters over a range of
 295 time scales, from intraseasonal to interannual.

296 Again, we assigned 40 possible linearly-spaced values for each of the sweep parameters, k_{\min} and c_{\max} ,
 297 and consider three combinations for the grazing parameters (m_Z , a_Z): (0.05, 1) (weak grazing); (0.015, 1)
 298 (intermediate grazing); and (0.015, 1.15) (strong grazing). We ran each simulation for 200 years and used
 299 the last 150 years for analysis. Figure 8 shows the dominant period of P_1^s for the three sweeps, in order
 300 of increasing grazing pressure, from left to right. Panel A shows that under weak grazing, the expected
 301 relationship between the sweep parameters and the succession time holds: larger values of c_{\max} and smaller
 302 values of k_{\min} lead to faster succession times. In the other two panels, the regions in white indicate that a
 303 dominant period never resolves due to aperiodicity. Most of the parameter space in panel C, where grazing
 304 is strongest, has dominant periods that never resolve.

305 5. Discussion and Conclusion

306 Partitioning the observed variability in planktonic ecosystems and community composition between in-
 307 trinsic and external sources is a difficult task. But a reasonable first step, which we have taken in this study,
 308 is to model one kind of variability (intrinsic, in our case) and the time scales on which it occurs. To do
 309 so, we developed and explored a zero-dimensional ecosystem model that describes a range of possible inter-
 310 actions between phytoplankton, nutrients, and zooplankton. The model supports two kinds of oscillations,
 311 which have been previously described in the literature and which we call R-oscillations and Z-oscillations.
 312 R-oscillations describe patterns of species succession, while Z-oscillations are predator-prey limit cycles of
 313 total biomass. Previous studies have incorporated one type of oscillation or the other into their models, but
 314 we are not aware of any that have studied them simultaneously. And there is a dearth of knowledge on the
 315 time scales of these oscillations in a realistic open ocean system.

316 We found that the species succession time for R-oscillations depends on the phytoplankton growth rates
317 at high and low nutrient concentrations. In our model, these depend strongly on two parameters: c_{\max} , which
318 controls the depletion rate of the nutrient in greatest abundance; and k_{\min} , which controls the growth rate
319 of the next phytoplankton species in line to invade and dominate the system. Over the range of parameters
320 in (6), we saw R-oscillations in the individual phytoplankton time series that ranged from roughly 100 to 900
321 days under predation-free conditions. Predator-prey Z-oscillations, on the other hand, consistently occurred
322 on time scales not exceeding 60 days. When the two kinds of oscillations interacted, R-oscillations became
323 even slower due to a top-down control on the rate of phytoplankton growth/nutrient depletion. And in the
324 aperiodic scenarios where the dominant period never resolves, distinct regimes emerged over decadal (or
325 longer) time scales.

326 The specific periods of oscillation and frequency of chaotic regime shifts are likely highly dependent
327 on the model parameters and structure. However, the wide range of time scales on which the community
328 structure and biomass varies is consistent with observations from laboratory data. The mesocosm experiment
329 from Benincà et al. (2008) mentioned in our introduction (Section 1) contains multiple time scales of variability
330 in species composition and biomass, and exhibits chaotic tendencies. While the structure of the food web
331 is different from our modeling experiment (it contains only two nutrients but additional compartments for
332 bacteria, detritus and detritivores), the results suggest that non-equilibrium dynamics play a key role in
333 shaping ecosystems. Our model examines this same idea via a particular set of mechanisms (namely R- and
334 Z-oscillations).

335 Though our model is suitable for this study in many ways, it also has some clear limitations. First,
336 only six phytoplankton species are included with two feeding strategies represented (small gleaners and large
337 opportunists), whereas there are tens of thousands of species in the real ocean with a continuum of sizes and
338 optimal growth conditions. Second, we assume that any intrinsic variability reflected in the data must be
339 attributed to one or two prescribed mechanisms. By design, we have omitted contributions to variability from
340 stochasticity in the environment, which may affect the evolution of biomass and community composition in
341 a nontrivial way, even in systems with minimal seasonality. We leave these avenues of investigation open for
342 future studies.

343 From the results above, we determined that intrinsic oscillations can occur on broad range of time scales.
344 These oscillations are not tied to any physical phenomena, such as seasonal changes in light or interannual
345 changes in environmental parameters, but they share overlap in their frequency ranges. Thus, we believe that
346 phytoplankton may exhibit complex responses to many external sources of variability. The degree to which
347 the nature of these responses diverges from the external variability will likely depend on the strength of the
348 forcings and the region of interest. At highly seasonal latitudes, R- and Z-oscillations would be inhibited
349 by winter mixing, which reduces predator-prey encounters and the amount of available light and nutrient.
350 Phytoplankton evolution may therefore be phase locked to seasonal changes, as reflected in SeaWiFS data
351 from the North Atlantic, for example in (Behrenfeld, 2010). The idea is also reflected in (Winder and Cloern,
352 2010), which contrasts a strong annual bloom for an ecosystem in the Wadden Sea (North Atlantic) with one
353 in Lake Hatchineha (Florida), whose blooms are irregular and occur on shorter time scales.

354 In contrast, coastal upwelling “hotspots” are characterized by a persistent inflow of nutrients from the

355 deep and elevated predatory pressure — conditions that are conducive to domination by intrinsic oscillations.
 356 Evidence of intrinsic long-term variability in coastal communities is also reflected in phytoplankton time
 357 series. [Bode et al. \(2015\)](#) found from the RADIALES dataset, collected off the northwest coast of the
 358 Iberian peninsula, that phytoplankton variability tends to be stochastic. Trends emerge over interannual and
 359 decadal time scales that do not correlate meaningfully with physical properties such as temperature and and
 360 stratification. [Cianelli et al. \(2017\)](#) also concluded that the structure of coastal ecosystems in the Gulf of
 361 Naples is primarily influenced by intrinsic factors, with physical contributions aiding biodiversity by diluting
 362 ecosystems and preventing dominance by a handful of species.

363 Another way to frame the above discussion is to ask how the amplitude of intrinsic variability compares
 364 to that of external variability under a variety of physical conditions. The oscillations in this study were quite
 365 large for both individual compartments (R-oscillations) and in total biomass (Z-oscillations). We expect that
 366 the presence of external oscillations will reduce the amplitude of the intrinsic contributions. But the degree
 367 to which this happens will depend on the strength of the relevant forcings. We intend to explore this open
 368 question in a follow-up study.

369 Acknowledgements

370 The authors thank Stephanie Dutkiewicz and Olivier Aumont for early feedback on this work. BM,
 371 KSS, and ML gratefully acknowledge support from the New York University Abu Dhabi Institute, through
 372 its Center for Prototype Climate Modeling. ML gratefully acknowledges support from TOSCA-CNES and
 373 ANR-SOBUMS (contract ANR-16-CE01-0014).

374 Appendix A. Simplified Model

375 Here, we present a simplified ecosystem model based on the equations outlined in Section 2. We include
 376 two nutrients R_1 and R_2 ; two small phytoplankton P_1 and P_2 ; and one zooplankton Z . We use the same
 377 symbols for our parameters, but we remove superscripts and abandon the concept of size classes.

The equations are

$$\frac{dR_1}{dt} = \tau(S_1 - R_1) - \mu \left[C_{11} \min \left\{ \frac{R_1}{K_{11} + R_1}, \frac{R_2}{K_{21} + R_2} \right\} P_1 + C_{12} \min \left\{ \frac{R_1}{K_{12} + R_1}, \frac{R_2}{K_{22} + R_2} \right\} P_2 \right], \quad (\text{A.1a})$$

$$\frac{dR_2}{dt} = \tau(S_2 - R_2) - \mu \left[C_{21} \min \left\{ \frac{R_1}{K_{11} + R_1}, \frac{R_2}{K_{21} + R_2} \right\} P_1 + C_{22} \min \left\{ \frac{R_1}{K_{12} + R_1}, \frac{R_2}{K_{22} + R_2} \right\} P_2 \right], \quad (\text{A.1b})$$

$$\frac{dP_1}{dt} = -\tau P_1 + \left[\mu \min \left\{ \frac{R_1}{K_{11} + R_1}, \frac{R_2}{K_{21} + R_2} \right\} - m_P - \frac{gZ}{K_Z + P_1 + P_2} \right] P_1, \quad (\text{A.1c})$$

$$\frac{dP_2}{dt} = -\tau P_2 + \left[\mu \min \left\{ \frac{R_1}{K_{12} + R_1}, \frac{R_2}{K_{22} + R_2} \right\} - m_P - \frac{gZ}{K_Z + P_1 + P_2} \right] P_2, \quad (\text{A.1d})$$

$$\frac{dZ}{dt} = -\tau Z + \frac{gZ}{K_Z + P_1 + P_2} (P_1 + P_2) - m_Z Z^2 \quad (\text{A.1e})$$

378 There are two nutrient currencies R_1 and R_2 , and we can convert from phytoplankton units (carbon) to
 379 nutrient units via multiplication by the stoichiometric coefficients C_{ji} . The stoichiometric coefficients for Z ,

380 which we may call C_j^Z , do not appear in the equations because zooplankton do not introduce a loss term to
381 the nutrient equations.

382 We can examine the evolution of ϕ_j , or the total amount of R_j in the system

$$\phi_1 = R_1 + C_{11}P_1 + C_{12}P_2 + C_1^Z Z \quad (\text{A.2a})$$

$$\phi_2 = R_2 + C_{21}P_1 + C_{22}P_2 + C_2^Z Z \quad (\text{A.2b})$$

383 If we differentiate ϕ_j in time, we have a balance between: nutrient inflow, outflow from all compartments,
384 and phytoplankton/zooplankton mortality

$$\frac{d\phi_1}{dt} = \tau(S_1 - \phi_1) - m_P(C_{11}P_1 + C_{12}P_2) - C_1^Z m_Z^2 \quad (\text{A.3a})$$

$$\frac{d\phi_2}{dt} = \tau(S_2 - \phi_2) - m_P(C_{21}P_1 + C_{22}P_2) - C_2^Z m_Z^2 \quad (\text{A.3b})$$

385 Note that these equations do not depend on growth or uptake terms, as these processes are completely
386 balanced and cancel upon adding up the right-hand sides of the equations.

387 References

388 Alvain, S., Moulin, C., Dandonneau, Y., Loisel, H., 2008. Seasonal distribution and succession of dominant
389 phytoplankton groups in the global ocean : A satellite view. *Global Biogeochemical Cycles* 22, 1–15.
390 doi:[10.1029/2007GB003154](https://doi.org/10.1029/2007GB003154).

391 Aumont, O., Maier-Reimer, E., Blain, S., Monfray, P., 2003. An ecosystem model of the global ocean including
392 Fe, Si, P colimitations. *Global Biogeochemical Cycles* 17. doi:[10.1029/2001gb001745](https://doi.org/10.1029/2001gb001745).

393 Aumont, O., Maury, O., Lefort, S., Bopp, L., 2018. Evaluating the Potential Impacts of the Diurnal Vertical
394 Migration by Marine Organisms on Marine Biogeochemistry. *Global Biogeochemical Cycles* 32, 1622–1643.
395 doi:[10.1029/2018GB005886](https://doi.org/10.1029/2018GB005886).

396 Aumont, O., Tagliabue, A., Bopp, L., Gehlen, M., 2015. PISCES-v2: an ocean biogeochemical model
397 for carbon and ecosystem studies. *Geoscientific Model Development* 8, 2465–2513. doi:[10.5194/
398 gmd-8-2465-2015](https://doi.org/10.5194/gmd-8-2465-2015).

399 Behrenfeld, M.J., 2010. Abandoning Sverdrup’s Critical Depth Hypothesis on phytoplankton blooms. *Ecology*
400 91, 977–989. URL: <http://www.esajournals.org/doi/abs/10.1890/09-1207.1>, doi:[10.1890/09-1207.
401 1](https://doi.org/10.1890/09-1207.1).

402 Behrenfeld, M.J., O’Malley, R.T., Siegel, D.A., McClain, C.R., Sarmiento, J.L., Feldman, G.C., Milligan,
403 A.J., Falkowski, P.G., Letelier, R.M., Boss, E.S., 2006. Climate-driven trends in contemporary ocean
404 productivity. *Nature* 444, 752–755. doi:[10.1038/nature05317](https://doi.org/10.1038/nature05317).

405 Benincà, E., Ballantine, B., Ellner, S.P., Huisman, J., 2015. Species fluctuations sustained by a cyclic succes-
406 sion at the edge of chaos. *Proceedings of the National Academy of Sciences of the United States of America*
407 112, 6389–94. URL: <http://www.ncbi.nlm.nih.gov/pubmed/25902520>[http://www.pubmedcentral.
408 nih.gov/articlerender.fcgi?artid=PMC4443354](http://www.pubmedcentral.nih.gov/articlerender.fcgi?artid=PMC4443354), doi:[10.1073/pnas.1421968112](https://doi.org/10.1073/pnas.1421968112).

409 Benincà, E., Huisman, J., Heerkloss, R., Johnk, K.D., Branco, P., Van Nes, E.H., Scheffer, M., Ellner, S.P.,
410 2008. Chaos in a long-term experiment with a plankton community. *Nature Letters* 451. doi:[10.1038/
411 nature06512](https://doi.org/10.1038/nature06512).

412 Blasius, B., Rudolf, L., Weithoff, G., Gaedke, U., Fussmann, G.F., 2019. Long-term cyclic persistence and
413 phase signature in an experimental predator-prey system. *Nature* , 1–36URL: [http://dx.doi.org/10.
414 1038/s41586-019-1857-0](http://dx.doi.org/10.1038/s41586-019-1857-0), doi:[10.1038/nature11356](https://doi.org/10.1038/nature11356).

415 Bode, A., Estévez, M.G., Varela, M., Vilar, J.A., 2015. Annual trend patterns of phytoplankton species
416 abundance belie homogeneous taxonomical group responses to climate in the NE Atlantic upwelling. *Marine
417 Environmental Research* 110, 81–91. doi:[10.1016/j.marenvres.2015.07.017](https://doi.org/10.1016/j.marenvres.2015.07.017).

418 Bopp, L., Resplandy, L., Orr, J.C., Doney, S.C., Dunne, J.P., Gehlen, M., Halloran, P., Heinze, C., Ilyina,
419 T., Séférian, R., Tjiputra, J., Vichi, M., 2013. Multiple stressors of ocean ecosystems in the 21st century:
420 Projections with CMIP5 models. *Biogeosciences* 10, 6225–6245. doi:[10.5194/bg-10-6225-2013](https://doi.org/10.5194/bg-10-6225-2013).

421 Carranza, M.M., Gille, S.T., 2014. Southern Ocean wind-driven entrainment enhances satellite chlorophyll-a
422 through the summer. *Journal of Geophysical Research: Oceans* , 2121–2128doi:[10.1002/jgrc.20224](https://doi.org/10.1002/jgrc.20224).

423 Chavez, F.P., Messi, M., Pennington, J.T., 2011. Marine Primary Production in Relation to Climate Vari-
424 ability and Change. *Annu. Rev. Mar. Sci.* 3, 227–60. doi:[10.1146/annurev.marine.010908.163917](https://doi.org/10.1146/annurev.marine.010908.163917).

425 Cianelli, D., D’Alelio, D., Uttieri, M., Sarno, D., Zingone, A., Zambianchi, E., D’Alcalà, M.R., 2017. Disen-
426 tangling physical and biological drivers of phytoplankton dynamics in a coastal system. *Scientific Reports*
427 7, 1–15. doi:[10.1038/s41598-017-15880-x](https://doi.org/10.1038/s41598-017-15880-x).

428 Cropp, R., Norbury, J., 2009. Parameterizing plankton functional type models: Insights from a dynamical
429 systems perspective. *Journal of Plankton Research* 31, 939–963. doi:[10.1093/plankt/fbp042](https://doi.org/10.1093/plankt/fbp042).

430 Dakos, V., Benincà, E., Van Nes, E.H., Philippart, C.J., Scheffer, M., Huisman, J., 2009. Interannual
431 variability in species composition explained as seasonally entrained chaos. *Proceedings of the Royal Society
432 B: Biological Sciences* 276, 2871–2880. doi:[10.1098/rspb.2009.0584](https://doi.org/10.1098/rspb.2009.0584).

433 Demarcq, H., Reygondeau, G., Alvain, S., Vantrepotte, V., 2012. Monitoring marine phytoplankton season-
434 ality from space. *Remote Sensing of Environment* 117, 211–222. URL: [http://dx.doi.org/10.1016/j.
435 rse.2011.09.019](http://dx.doi.org/10.1016/j.rse.2011.09.019), doi:[10.1016/j.rse.2011.09.019](https://doi.org/10.1016/j.rse.2011.09.019).

436 d’Ovidio, F., De Monte, S., Alvain, S., Dandonneau, Y., Lévy, M., 2010. Fluid dynamical niches of phyto-
437 plankton types. *Proceedings of the National Academy of Sciences of the United States of America* 107,
438 18366–18370. doi:[10.1073/pnas.1004620107](https://doi.org/10.1073/pnas.1004620107).

439 Dutkiewicz, S., Follows, M.J., Bragg, J.G., 2009. Modeling the coupling of ocean ecology and biogeochemistry.
440 *Global Biogeochemical Cycles* 23. URL: <http://doi.wiley.com/10.1029/2008GB003405>, doi:[10.1029/
441 2008GB003405](https://doi.org/10.1029/2008GB003405).

442 Dutkiewicz, S., Hickman, A.E., Jahn, O., Henson, S., Beaulieu, C., Monier, E., 2019. Ocean colour
443 signature of climate change. *Nature Communications* 10. URL: [http://dx.doi.org/10.1038/
444 s41467-019-08457-x](http://dx.doi.org/10.1038/s41467-019-08457-x), doi:10.1038/s41467-019-08457-x.

445 Edwards, A.M., Brindley, J., 1996. Oscillatory behaviour in a three-component plankton population model.
446 *Dynamical Systems* 11, 347–370. doi:10.1080/02681119608806231.

447 Fasham, M.J., Ducklow, H.W., McKelvie, S.M., 1990. A nitrogen-based model of plankton dynamics in the
448 oceanic mixed layer. *Journal of Marine Research* 48, 591–639. doi:10.1357/002224090784984678.

449 Fauchereau, N., Tagliabue, A., Bopp, L., Monteiro, P.M., 2011. The response of phytoplankton biomass
450 to transient mixing events in the Southern Ocean. *Geophysical Research Letters* 38, 1–6. doi:10.1029/
451 2011GL048498.

452 Follows, M.J., Dutkiewicz, S., Grant, S., Chisholm, S.W., 2007. Emergent biogeography of microbial com-
453 munities in a model ocean. *Science (New York, N.Y.)* 315, 1843–6. URL: [http://www.ncbi.nlm.nih.
454 gov/pubmed/17395828](http://www.ncbi.nlm.nih.gov/pubmed/17395828), doi:10.1126/science.1138544.

455 Fussmann, G.F., Ellner, S.P., Shertzer, K.W., Hairston N.G., J., 2000. Crossing the hopf bifurcation in a
456 live predator-prey system. *Science* 290, 1358–1360. doi:10.1126/science.290.5495.1358.

457 Gilpin, M.E., 1979. Spiral Chaos in a Predator-Prey Model. *The American Naturalist* 113, 306–308.

458 Gotthlich, L., Oshlies, A., 2015. Disturbance characteristics determine the timescale of competitive exclusion
459 in a phytoplankton model. *Ecological Modelling* 296, 126–135. URL: [http://dx.doi.org/10.1016/j.
460 ecolmodel.2014.10.033](http://dx.doi.org/10.1016/j.ecolmodel.2014.10.033), doi:10.1016/j.ecolmodel.2014.10.033.

461 Hastings, A., 2020. Long-term predator-prey cycles finally achieved in the lab. doi:10.1038/
462 d41586-019-03603-3.

463 Hindmarsh, A.C., 1982. ODEPACK, A Systematized Collection of ODE Solvers. *IMACS Transactions on*
464 *Scientific Computation* 1, 55–64.

465 Huisman, J., Pham Thi, N.N., Karl, D.M., Sommeijer, B., 2006. Reduced mixing generates oscillations and
466 chaos in the oceanic deep chlorophyll maximum. *Nature* 439, 322–325. doi:10.1038/nature04245.

467 Huisman, J., Weissing, F.J., 1999. Biodiversity of plankton by species oscillations and chaos. *Nature* 402,
468 407–410. doi:10.1038/46540.

469 Huisman, J., Weissing, F.J., 2001. Biological conditions for oscillations and chaos generated by multi-
470 species competition. *Ecology* 82, 2682–2695. URL: [http://doi.wiley.com/10.1890/0012-9658\(2001\)
471 082\[2682:BCFOAC\]2.0.CO;2](http://doi.wiley.com/10.1890/0012-9658(2001)082[2682:BCFOAC]2.0.CO;2), doi:10.1890/0012-9658(2001)082[2682:BCFOAC]2.0.CO;2.

472 Keerthi, M.G., Levy, M., Aumont, O., Lengaigne, M., Antoine, D., 2020. Contrasted Contribution of In-
473 traseasonal Time Scales to Surface Chlorophyll Variations in a Bloom and an Oligotrophic Regime. *Journal*
474 *of Geophysical Research: Oceans* 125. doi:10.1029/2019jc015701.

475 Klausmeier, C.A., Litchman, E., Daufresne, T., Levin, S., 2004. Optimal nitrogen-to-phosphorus stoichiometry of phytoplankton. *Nature* 429, 171–174. doi:1.1029/2001GL014649.

476

477 Lévy, M., Franks, P.J., Smith, K.S., 2018. The role of submesoscale currents in structuring marine ecosystems. *Nature communications* 9, 4758. doi:10.1038/s41467-018-07059-3.

478

479 Mahadevan, A., D’Asaro, E., Lee, C., Perry, M.J., 2012. Eddy-driven stratification initiates North Atlantic spring phytoplankton blooms. *Science (New York, N.Y.)* 337, 54–8. URL: <http://www.sciencemag.org/content/337/6090/54.abstract>, doi:10.1126/science.1218740.

480

481

482 Martinez, E., Antoine, D., Ortenzio, F.D., Gentili, B., 2009. Climate-Driven Basin-Scale Decadal Oscillations of Oceanic Phytoplankton. *Science* 1253. doi:10.1126/science.1177012.

483

484 Mayot, N., D’Ortenzio, F., Uitz, J., Gentili, B., Ras, J., Vellucci, V., Golbol, M., Antoine, D., Claustre, H., 2017. Influence of the Phytoplankton Community Structure on the Spring and Annual Primary Production in the Northwestern Mediterranean Sea. *Journal of Geophysical Research: Oceans* 122, 9918–9936. doi:10.1002/2016JC012668.

485

486

487

488 Menkes, C.E., Lengaigne, M., Lévy, M., Ethé, C., Bopp, L., Aumont, O., Vincent, E., Vialard, J., Jullien, S., 2016. Global impact of tropical cyclones on primary production. *Global Biogeochemical Cycles* 29, 767–786. doi:10.1002/2015GB005214.Received.

489

490

491 Messié, M., Chavez, F.P., 2017. Nutrient supply, surface currents, and plankton dynamics predict zooplankton hotspots in coastal upwelling systems. *Geophysical Research Letters* 44, 8979–8986. URL: <https://onlinelibrary.wiley.com/doi/full/10.1002/2017GL074322>, doi:10.1002/2017GL074322.

492

493

494 Messié, M., Ledesma, J., Kolber, D.D., Michisaki, R.P., Foley, D.G., Chavez, F.P., 2009. Progress in Oceanography Potential new production estimates in four eastern boundary upwelling ecosystems. *Progress in Oceanography* 83, 151–158. URL: <http://dx.doi.org/10.1016/j.pocean.2009.07.018>, doi:10.1016/j.pocean.2009.07.018.

495

496

497

498 Millman, K.J., Aivazis, M., 2011. Python for scientists and engineers. doi:10.1109/MCSE.2011.36.

499

500

501 Petzold, L., 1983. Automatic selection of methods for solving stiff and nonstiff systems of ordinary differential equations. *SIAM Journal on Scientific and Statistical Computing* 4, 136–148.

502

503

504

505 Platt, T., White, G.N., Zhai, L., Sathyendranath, S., Roy, S., 2009. The phenology of phytoplankton blooms: Ecosystem indicators from remote sensing. *Ecological Modelling* 220, 3057–3069. URL: <https://www.sciencedirect-com.proxy.library.nyu.edu/science/article/pii/S0304380008005462>, doi:10.1016/J.ECOLMODEL.2008.11.022.

506

507

508 Poggiale, J., Eynaud, Y., Baklouti, M., 2013. Impact of periodic nutrient input rate on trophic chain properties. *Ecological Complexity* 14, 56–63. URL: <http://dx.doi.org/10.1016/j.ecocom.2013.01.005>, doi:10.1016/j.ecocom.2013.01.005.

508 Prowe, A.E., Pahlow, M., Dutkiewicz, S., Oschlies, A., 2014. How important is diversity for capturing
509 environmental-change responses in ecosystem models? *Biogeosciences* 11, 3397–3407. doi:[10.5194/
510 bg-11-3397-2014](https://doi.org/10.5194/bg-11-3397-2014).

511 Redfield, A.C., 1934. On the proportions of organic derivatives in sea water and their relation to the
512 composition of plankton. University Press of Liverpool.

513 Resplandy, L., Vialard, J., Lévy, M., Aumont, O., Dandonneau, Y., 2009. Seasonal and intraseasonal biogeo-
514 chemical variability in the thermocline ridge of the southern tropical Indian Ocean. *Journal of Geophysical
515 Research: Oceans* 114, 1–13. doi:[10.1029/2008JC005246](https://doi.org/10.1029/2008JC005246).

516 Rousseaux, C.S., Gregg, W.W., 2015. Recent decadal trends in global phytoplankton composition. *Global
517 Biogeochemical Cycles* , 1674–1688doi:[10.1002/2015GB005139](https://doi.org/10.1002/2015GB005139).Received.

518 Salgado-Hernanz, P.M., Racault, M.F., Font-Muñoz, J.S., Basterretxea, G., 2019. Trends in phytoplankton
519 phenology in the Mediterranean Sea based on ocean-colour remote sensing. *Remote Sensing of Environment*
520 221, 50–64. URL: <https://doi.org/10.1016/j.rse.2018.10.036>, doi:[10.1016/j.rse.2018.10.036](https://doi.org/10.1016/j.rse.2018.10.036).

521 Sarmiento, J.L., Slater, R.D., Fasham, M.J.R., Ducklow, H.W., Toggweiler, J.R., Williams, R., 1993. A
522 seasonal three-dimensional ecosystem model of nitrogen cycling in the North Atlantic euphotic zone: A
523 comparison of model results with observations from Bermuda Station “S” and OWS “India.”. *Glob. Bio-
524 geochem. Cycles* 7, 379.

525 Sathyendranath, S., Ji, R., Browman, H.I., 2015. Revisiting Sverdrup’s critical depth hypothesis. *ICES
526 Journal of Marine Science* 72, 1892–1896. doi:[10.1093/icesjms/fsv110](https://doi.org/10.1093/icesjms/fsv110).

527 Thomalla, S.J., Fauchereau, N., Swart, S., Monteiro, P.M., 2011. Regional scale characteristics of the seasonal
528 cycle of chlorophyll in the Southern Ocean. *Biogeosciences* 8, 2849–2866. doi:[10.5194/bg-8-2849-2011](https://doi.org/10.5194/bg-8-2849-2011).

529 Tilman, D., 1977. Resource Competition between Plankton Algae: An Experimental and Theoretical Ap-
530 proach. *Ecology* 58, 338–348.

531 Tilman, D., 1985. The Resource-Ratio Hypothesis of Plant Succession. *The American Naturalist* 125, 827–
532 852.

533 Vantrepotte, V., Mélin, F., 2011. Inter-annual variations in the SeaWiFS global chlorophyll a concentration
534 (1997-2007). *Deep-Sea Research Part I: Oceanographic Research Papers* 58, 429–441. doi:[10.1016/j.dsr.
535 2011.02.003](https://doi.org/10.1016/j.dsr.2011.02.003).

536 Winder, M., Cloern, J.E., 2010. The annual cycles of phytoplankton biomass. *Philosophical Transactions of
537 the Royal Society B: Biological Sciences* 365, 3215–3226. URL: [http://rstb.royalsocietypublishing.
538 org/cgi/doi/10.1098/rstb.2010.0125](http://rstb.royalsocietypublishing.org/cgi/doi/10.1098/rstb.2010.0125), doi:[10.1098/rstb.2010.0125](https://doi.org/10.1098/rstb.2010.0125).